Martin Oelschlägel*, Tobias Meyer, Gabriele Schackert, Matthias Kirsch, Stephan B. Sobottka and Ute Morgenstern

Intraoperative optical imaging of metabolic changes after direct cortical stimulation – a clinical tool for guidance during tumor resection?

https://doi.org/10.1515/bmt-2017-0156
Received September 1, 2017; accepted October 24, 2017; online first February 5, 2018

Abstract: Brain tumor resection is even today one of the most challenging disciplines in neurosurgery. The current state of the art for the identification of tumor tissue during the surgical procedure comprises a wide variety of different tools, each with its own limitations and drawbacks. In this paper, we present a novel approach, the use of optical imaging in connection with direct electrical cortical stimulation (DCS), for identification of impaired tumor tissue and functional intact normal brain tissue under intraoperative conditions. Measurements with an optical imaging setup were performed as a proof of concept on three patients who underwent tumor resection of superficial gliomas. Direct electrical stimulations were applied on tumor tissue and surrounding brain tissue in each patient and characteristic features from the observed changes in the optical properties were compared between the different groups. The results reveal that in all patients a differentiation between non-functional tumor tissue and functional intact brain tissue was possible, and the technique might be a useful clinical tool in the future.

Keywords: brain tumor surgery; cortical mapping; direct cortical stimulation; optical imaging.

***Corresponding author: Martin Oelschlägel,** Faculty of Electrical and Computer Engineering, Technische Universität Dresden, Institut für Biomedizinische Technik, D – 01307 Dresden, Germany, Phone: +49 351 463 32118, Fax: +49 351 463 36026,
E-mail: martin.oelschlaegel@tu-dresden.de
Tobias Meyer: Institute of Biomedical Engineering, Faculty of Electrical and Computer Engineering, Technische Universität Dresden, 01307 Dresden, Germany; and ABX-CRO Advanced Pharmaceutical Services Forschungsgesellschaft m.b.H., 01307 Dresden, Germany
Gabriele Schackert, Matthias Kirsch and Stephan B. Sobottka: Department of Neurosurgery, Faculty of Medicine Carl Gustav Carus, Technische Universität Dresden, 01307 Dresden, Germany
Ute Morgenstern: Institute of Biomedical Engineering, Faculty of Electrical and Computer Engineering, Technische Universität Dresden, 01307 Dresden, Germany

Introduction

Brain tumor resection, even with today's modern imaging modalities, is one of the most challenging disciplines in neurosurgery. The outcome and progression free survival for the patient is directly linked to the extent of tumor resection [9, 10, 14]. The current state of the art for the guidance and orientation of the surgeon during the tumor resection process comprises a wide variety of different tools including neuronavigation based on preoperative acquired magnetic resonance imaging (MRI), dye imaging (e.g. 5-aminolevulinic acid fluorescence), intraoperative ultrasound, functional mapping and the more sophisticated approaches such as diffusion tensor imaging (DTI) and intraoperative MRI. Each of the mentioned methods has its own individual drawbacks and limitations. Neuronavigation suffers from brain shift after craniotomy and ongoing loss of accuracy during the surgical intervention [13]. Dye imaging is bound to specific types of tumor tissue, intraoperative MRI is time consuming and still not available in all countries and the functional mapping procedures are only applicable if the surgeon operates within specific regions of the brain or if the patient is awake. Direct electrical cortical stimulation (commonly used abbreviations are DES, DECS or DCS) is one tool that is already used to a large extent in neurosurgery for brain mapping and functional preserving as it is able to trigger (or suppress) neuronal activity and therefore perform specific functions, e.g. language [1, 2]. Nevertheless, the feedback from the awake patient is essential in mapping of higher cognitive function during the procedure. In the past, several groups showed the feasibility, the practicability and the potential use cases of optical imaging within the clinical environment [4, 5]. Our own group refined the intraoperative optical imaging technique (IOI) especially for robust identification of functional areas under intraoperative conditions with peripheral stimulation [7, 8, 11, 12]. Especially in connection with direct cortical stimulation, Suh et al. [15] demonstrated that changes in optical properties of the cortical surface can be observed with optical imaging

even under general anesthesia in the patient. In this work, we focused on investigating whether the combination of IOI and DCS might be a useful intraoperative tool for differentiation and delineation between tumor and non-tumor tissue. Therefore, we performed proof-of-concept measurements on patients who underwent resection of superficial gliomas. A mapping of bipolar direct cortical stimulations was performed over the whole exposed surface in each patient and the observed, time-resolved changes in the cortical optical properties were compared between tumor and non-tumor tissue, respectively tumor and non-tumor stimulation sites.

Patients and methods

Patient characteristics

Measurements were performed after obtaining consent from the three patients who underwent resection of superficial gliomas. The study was approved by the Ethics Committee of the Medical Faculty, Technische Universität Dresden. Age, gender and histological information of each patient are shown in Table 1. Electrocortical stimulation was performed and supervised according to clinical standards by an experienced neurosurgeon and electrophysiologist.

Intraoperative stimulation and image acquisition

The exposed cortical surface of each patient was directly electrically stimulated ($I_{Stim} = 2–6$ mA, $T_{Stim} = 5$ s) with a bipolar electrode, driven by a standard neuro-stimulation device (Nicolet Biomedical, Madison, WI, USA). The direct electrical stimulations were performed on different stimulation sites, including suspected tumor tissue as well as tissue that was morphologically unsuspicious and therefore considered as functionally intact. Image data of each direct electrical stimulation were acquired with a charge-coupled device (CCD) camera (AxioCam MRm, Carl Zeiss MicroImaging, Jena, Germany, 4 fps, 2×2 binning mode, 692×520 pixels) attached via a beam splitter (50/50 Carl Zeiss Meditec AG, Jena, Germany) to a surgical microscope (OPMI Pico, Carl Zeiss Meditec AG, Germany). Light wavelength filtering was performed within the optical path of the camera near an isosbestic point of hemoglobin absorption (band-pass interference filter, $\lambda = 568 \pm 5$ nm, Edmund Optics, Mainz, Germany), focusing on cerebral blood volume changes (ΔCBV). Illumination was performed through the surgical microscope-integrated 180 W xenon lamp. For each stimulation site, image data of a 30-s rest period, 5-s stimulation period and 85-s poststimulus period were acquired from the cortical surface, resulting in a total dataset length of 120 s for each stimulation process.

Table 1: Patient characteristics.

	Age	Sex	Pathology	Tumor localization	No. of stimulations
Patient 01	39	♀	Astrocytoma WHO °II–III	Frontal	6
Patient 02	66	♂	Astrocytoma WHO °II–III	Frontal	7
Patient 03	19	♂	Glioblastoma	Parietal	6

Classification of stimulation sites

In the first step, the tumor volume as well as prominent anatomical structures (e.g. precentral and postcentral gyrus) were segmented in the preoperatively acquired MRI (T1-weighted) of each patient, which was also used for neuronavigation during the surgical procedure. Furthermore, the borders of the skull trepanation were marked, according to intraoperative captured neuronavigation points (see Figure 1A). The second step comprised the manual fusion of the IOI image and the MRI data based on the identified anatomical structures and other prominent landmarks like large vessels. Each position of the stimulating electrodes was marked in the IOI image data sets (see Figure 1B and D). The exact delineation of the tumor border was based on a postresectional image, which was acquired with the microscope-integrated camera by the neurosurgeon (see Figure 1C). This information was merged in the third step with the previous information. The classification of each electrode position was based on the results of the image fusion (see Figure 1D) and comprised three groups: tumor tissue, non-tumor tissue and the intermediary border. The border group classification was used, when the postoperative analysis revealed that within the region of interest (ROI), from which the time course was extracted (see below), tumor as well as non-tumor tissue were included.

Image processing, time course extraction and time course modeling

Postoperative image registration of each data set was performed to correct for motion of the cortical surface caused by heartbeat and respiration. Therefore an elastic registration based on Demon's algorithm was used [16]. The time-resolved light intensity changes were extracted from image data series, using for each frame a spatial pixel intensity value averaging over a circular ROI. The ROI was centered on each electrode tip position, with a radius of half of the interelectrode distance (see Figure 2). As the intensity of the reflected light from the vessels in the wavelength band of 568 ± 5 nm was very low, due to the high hemoglobin absorption, a vessel segmentation was performed for signal-to-noise ratio (SNR) enhancement. The vessel segmentation was done according to Frangi's method [3]. The intensity time courses within each ROI were then extracted only from the parts that were not segmented as vessels. Furthermore, specular reflections were excluded by using a threshold-based reflection segmentation over time. The time-resolved relative reflectance change $\frac{\Delta R}{R}(t)$ was calculated from the intensity time course $I(t)$ and the

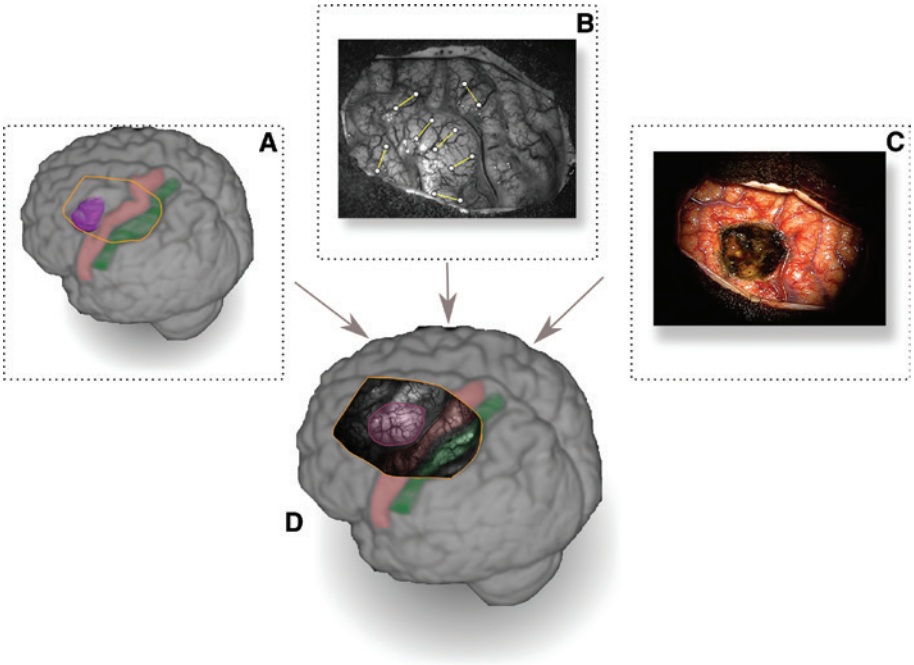

Figure 1: Fusion of multimodal imaging information for classification of different stimulation sites.
(A) Three-dimensional reconstruction of brain surface based on preoperatively acquired MRI data with segmentation of postcentral gyrus (somatosensory cortex, green), precentral gyrus (motor cortex, red) and tumor volume (purple); orange line shows trepanation. (B) Image of the trepanned area, acquired before resection by AxioCam MRm, superimposed with the different stimulation sites. White dots, connected by a yellow line, represent the position of the bipolar electrode tips during the single stimulation. (C) Image of the trepanned area acquired after tumor resection by a surgical microscope camera. (D) Image from Figure 1B merged with preoperative MRI from Figure 1A and segmented tumor borders based on Figure 1C.

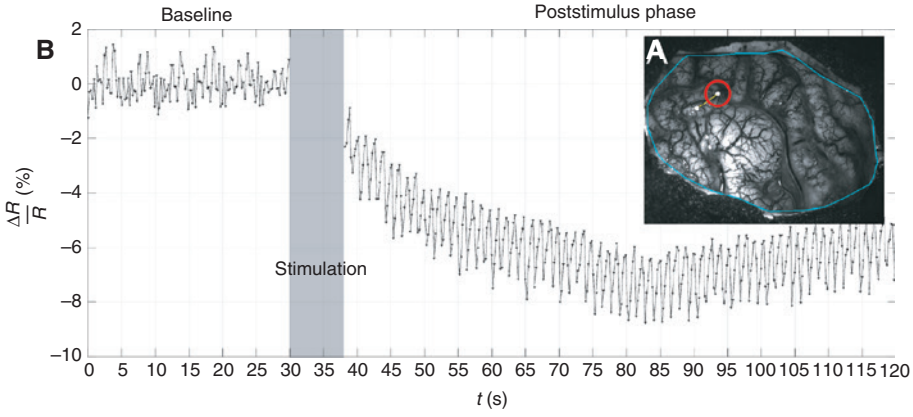

Figure 2: Extraction of time course from image data.
(A) White light image of the cortical surface acquired with AxioCam MRm (568 ± 5 nm), patient 01. Circular ROI for time course extraction of one exemplary electrode tip position is shown in red. (B) Mean time course of intensity within ROI corresponding to (A). According to image acquisition protocol, the time course starts with 30 s baseline condition, followed by around 5 s of bipolar stimulation and 85 s of stimulation answer. The intensity change during the electrical stimulation is not evaluable as the movement of the bipolar electrode to and from the stimulation site through the camera's field of view covers the cortical surface during this time period and leads to artifacts.

mean of baseline intensity time course $\overline{I}_{\text{base}}$ for each distinct point in time according to formula 1.

$$\left.\frac{\Delta R}{R}(t)\right|_{t=t_i} = \frac{I(t)\big|_{t=t_i} - \overline{I}_{\text{base}}}{\overline{I}_{\text{base}}} \cdot 100 \qquad (1)$$

In patient 03, stimulations were performed using altered stimulation current amplitudes. The resulting time courses were fitted by third-order polynomials to visually emphasize the actual low frequent changes due to hemodynamic response and to exclude the high frequency components induced by heartbeat and respiration that were present even after image registration.

ROI characteristics and time course feature extraction

From the mean ROI time course of the relative reflectance change of the poststimulus period $\overline{\frac{\Delta R_{ps}}{R}}(t)$, two features were calculated. The first one is the minimum of the measured signal

$$\widehat{\frac{\Delta R}{R}} = \min\left(\overline{\frac{\Delta R_{ps}}{R}}(t)\right). \tag{2}$$

Due to neurovascular coupling, the stimulation leads to an increase in blood volume and the cortical reflectance decreases with respect to the baseline. Therefore, this parameter correlates with the amount of increasing blood volume in the observed region. The second calculated feature is the integral

$$A_{ps} = \int_{t1}^{t2} \overline{\frac{\Delta R_{ps}}{R}}(t)\, dt \quad t1,t2\ldots\text{start / end point of the poststimulus period} \tag{3}$$

over the relative reflectance change for the whole poststimulus observation period. This parameter indicates, on the one hand, if the blood volume change that has been observed is an increase or decrease, and, on the other hand, how strong and respectively how long lasting those changes were. Due to integration the measure for this parameter is percentage change (of reflectance change) multiplied by time duration in seconds. Both time course features were compared between the classified stimulation sites, respectively ROIs.

Relative difference imaging

To visualize the spatial extent of the changes in optical cortical properties, a difference image calculation was performed. Therefore, a baseline mean image $\overline{I_{\text{base}}}$ was calculated and the difference toward a mean poststimulation phase image $\overline{I_{ps}}$ was calculated according to:

$$I_{\text{diff}} = \frac{\overline{I_{ps}} - \overline{I_{\text{base}}}}{\overline{I_{\text{base}}}} \tag{4}$$

with

$$\overline{I_{\text{base}_{xy}}} = \frac{\sum_i I_{i_{xy}}}{n_{\text{base}}} \quad i / n_{\text{base}} \ldots \text{index / number of baseline images} \tag{5}$$

and

$$\overline{I_{ps_{xy}}} = \frac{\sum_i I_{i_{xy}}}{n_{ps}} \quad i / n_{ps} \ldots \text{index / number of poststimulation phase images.} \tag{6}$$

The mean baseline image was typically calculated from images acquired 15 s prior to the start of stimulation, whereas the poststimulation mean image was calculated typically from images that were acquired 15 s after the end of stimulation.

Results

The comparison of the calculated time course features is shown for each group in Figure 3. Highly significant differences between the non-tumor tissue and tumor tissue groups were observed in both of the calculated time course features (Wilcoxon rank-sum test, $p < 0.001$). The absolute difference of the $\widehat{\frac{\Delta R}{R}}$ median for the non-tumor

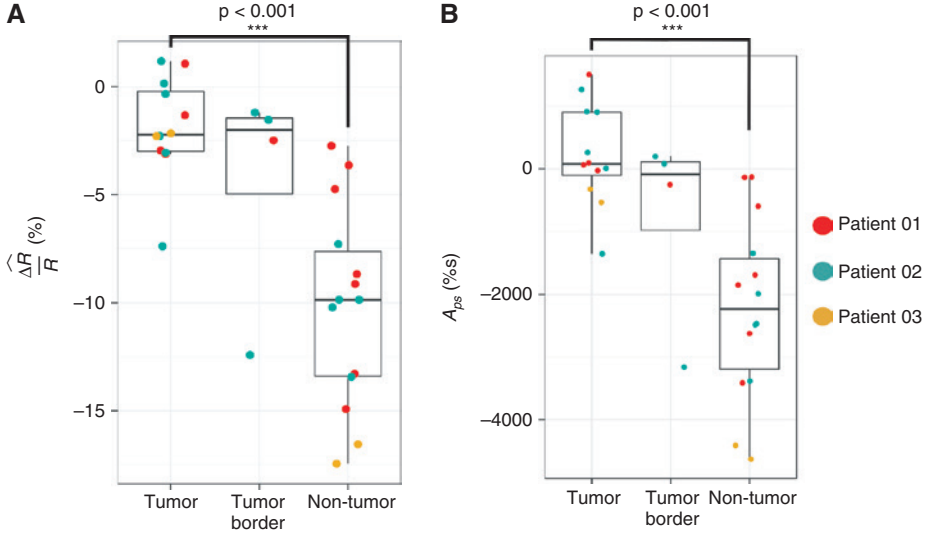

Figure 3: Minimum of measured reflectance change $\widehat{\frac{\Delta R}{R}}$ (A) and the integral over measured reflectance change A_{ps} (B) for all stimulations with $I_{\text{Stim}} = 6$ mA compared between tumor, non-tumor and tumor border stimulation sites.
(A) Tumor: $\tilde{x} = -2.2\%$, $Q_1 = -0.2\%$, $Q_3 = -3.0\%$, $n = 12$; tumor border: $\tilde{x} = -2.0\%$, $Q_1 = -1.5\%$, $Q_3 = -5.0\%$, $n = 4$; functional: $\tilde{x} = -9.9\%$, $Q_1 = -7.6\%$, $Q_3 = -13.3\%$, $n = 14$; (B) tumor: $\tilde{x} = 76\%$s, $Q_1 = 903\%$s, $Q_3 = -105\%$s; tumor border: $\tilde{x} = -88\%$s, $Q_1 = 108\%$s, $Q_3 = -980\%$s; functional: $\tilde{x} = -2229\%$s, $Q_1 = -1436\%$s, $Q_3 = -3192\%$s.

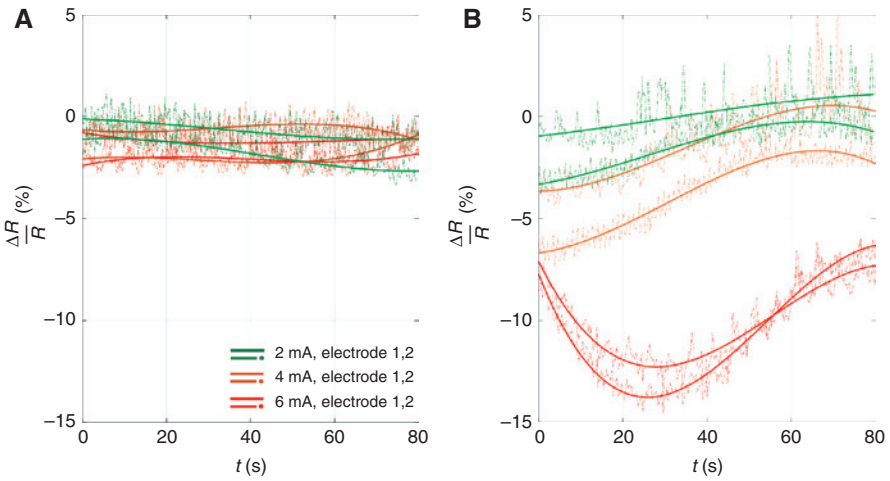

Figure 4: Raw data (dotted lines) and cubic fits (solid lines) for time courses extracted after repeated stimulation of the same stimulation site for tumor and non-tumor tissue in patient 03.
The stimulations were performed and acquired one after the other with decreasing current (I_{Stim} = 6 mA, I_{Stim} = 4 mA, I_{Stim} = 2 mA) in (A) tumor tissue and (B) non-tumor tissue.

and tumor tissue groups was 7.7%, and the absolute difference of the A_{ps} median of both groups was 2305%s. In patient 03, stimulations were performed with decreasing stimulation current (6 mA, 4 mA, 2 mA) for one tumor site as well as one non-tumor site. The resulting time courses were fitted by cubic polynomials which are shown in Figure 4A for tumor tissue and in Figure 4B for non-tumor tissue. In non-tumor tissue, an increasing stimulation current leads to an increase in the triggered ΔCBV, respectively $\widehat{\frac{\Delta R}{R}}$ (~–2% at 2 mA, ~–5% at 4 mA, ~–13% at 6 mA) and to a prolongation of the duration of the changes in the cortical optical properties. At 2 mA and 4 mA stimulation current, the amplitude maximum $\widehat{\frac{\Delta R}{R}}$ of the reflectance change is reached within the 5 s after the onset of stimulation. Therefore, the slope of the cubic fits in Figure 4B is already positive at the start of the shown poststimulus phase. Using a stimulation current of 6 mA, the slope of the fits is negative and $\widehat{\frac{\Delta R}{R}}$ is reached about 25 s after the end of stimulation, respectively 30 s after the onset of stimulation. Figure 5 shows the spatial distribution of the area where changes in the optical properties were detected for patient 03, using the relative difference image calculation described in the method section. On non-tumor tissue (see Figure 5A–C) the spatial extent of the area with changes in optical cortical properties increases with increasing stimulation current, especially with a stimulation current of 6 mA, remote effects are visible. On tumor tissue (see Figure 5D–F) virtually no changes in CBV are visible after stimulation, regardless of the used stimulation current amplitude. The results of the time-resolved analysis of the affected area for the non-tumor stimulations are shown in Figure 6. Different averaging time periods with a distance of 10 s between each were used for difference image calculation. The stimulation with 6 mA led to longest-lasting CBV changes, which were persistent during the full recording duration. With 4 mA stimulation current after ~45 to 60 s, most of the CBV changes are decayed, and with 2 mA already after ~25 to 45 s, the stimulation-induced effects are not discernible. Independent of current strength, the peak of stimulation-induced response was reached immediately after stimulation end.

Discussion

The results reveal significant differences in DCS responsiveness between tumor and non-tumor regions. In non-tumor classified tissue, the electrical stimulation-induced CBV changes are higher in amplitude and longer in duration. The evaluation of the A_{ps} parameter shows that in tumor areas, especially in patient 01 and patient 02, predominantly an increase in luminance (reduced CBV) after electrical stimulation was observed. This is controversial to the expected behavior of functional tissue: decrease in luminance resulting from an increase in blood volume. An explanation for this finding might be that due to the electrical stimulation, nearby areas, which still have an intact neurovascular coupling, are excited, and blood volume is

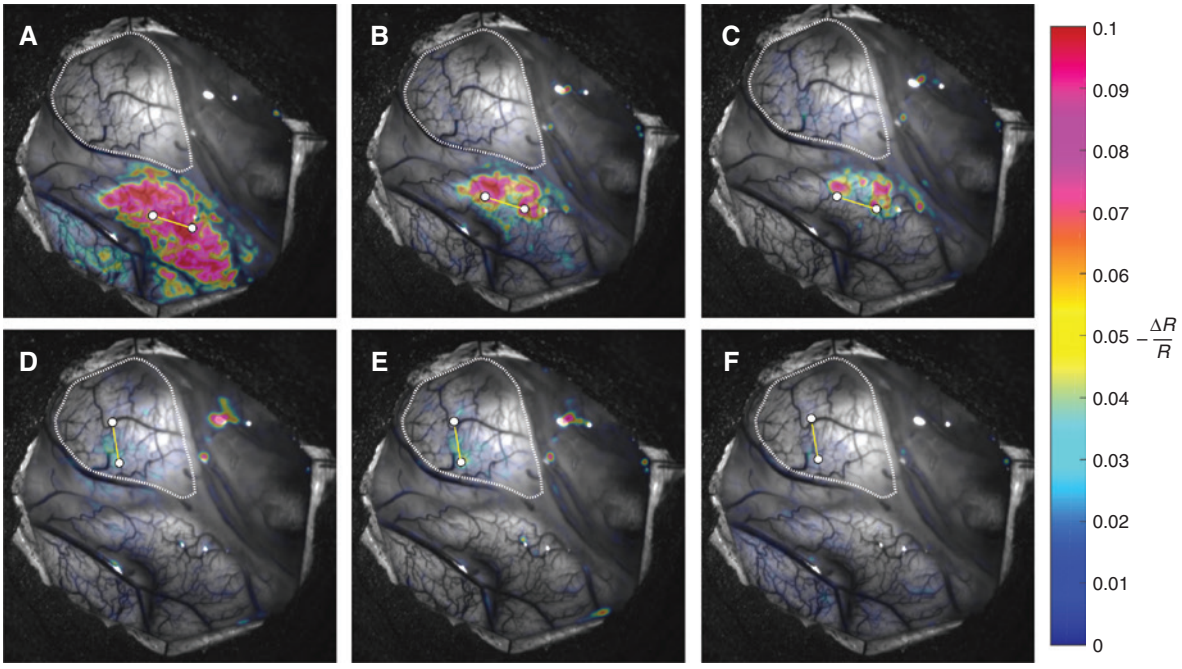

Figure 5: Fusion of white light image and relative difference image for stimulations with different stimulation currents.
The relative difference image is shown color coded between 0% and 10% reflectance decrease and overlaid with transparency.
(A) $I_{Stim} = 6$ mA, non-tumor tissue. (B) $I_{Stim} = 4$ mA, non-tumor tissue. (C) $I_{Stim} = 2$ mA, non-tumor tissue. (D) $I_{Stim} = 6$ mA, tumor tissue.
(E) $I_{Stim} = 4$ mA, tumor tissue. (E) $I_{Stim} = 2$ mA, tumor tissue. Dotted line represents the tumor segmentation border.

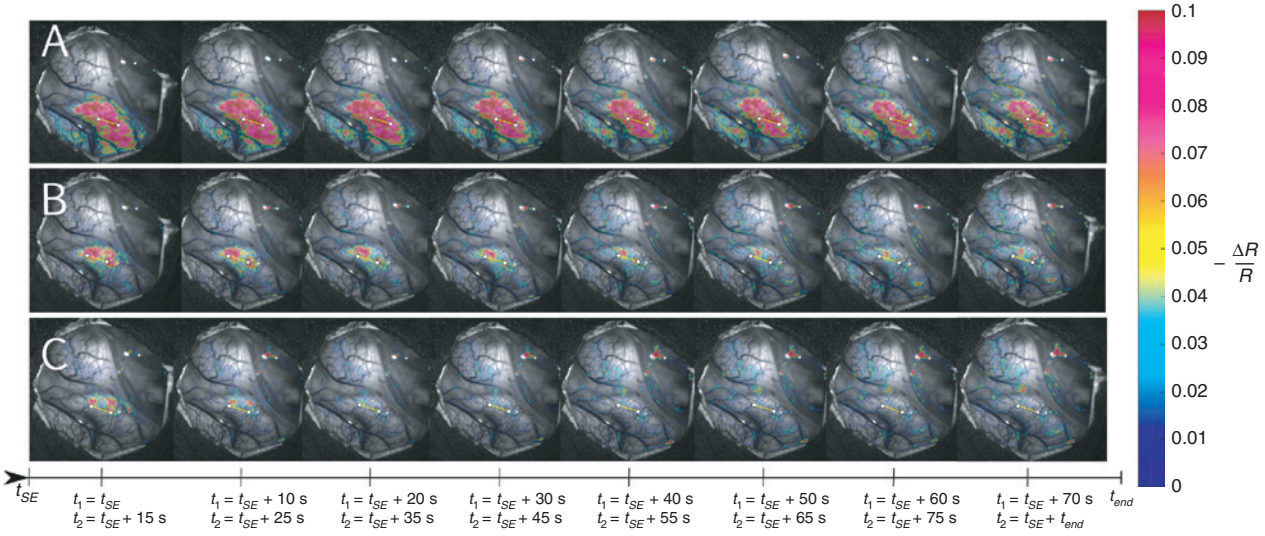

Figure 6: Time-resolved visualization of electrical stimulation-affected area for non-tumor stimulation sites in patient 03 using the relative difference imaging technique.
(A) $I_{Stim} = 6$ mA. (B) $I_{Stim} = 4$ mA. (C) $I_{Stim} = 2$ mA. Images were created by shifting the averaging time periods for calculation of $\overline{I_{ps}}$. Time period start (t_1) and end points (t_2) for calculation are shown in the figure.

shifted out of the impaired stimulation area around the electrode towards those regions. A more technical explanation for this phenomenon might be the influence of reflections. Even though pixels, which reach 95% of their saturation value in course of time, were excluded from averaging, the influence of reflections cannot be completely compensated, as the blooming effect might lead to an increase in luminance of adjacent regions which are not segmented by this threshold. In-depth investigations, especially on technical disturbances, should be included

in future work. The detailed evaluation of stimulations with altered stimulation current amplitude in patient 03 reveals considerable differences between the extents of the regions that are affected by electrical stimulation. Whereas a stimulation current of 2 mA affected only a small area around the electrode tips, an increase to 6 mA led already to extensive changes and moreover possibly remote effects. The current-altered stimulations on suspected tumor tissue in comparison were not able to trigger an increase in CBV. This is visible in the visualization of the spatial extent of activation as well as in the cubic fits of the time courses that were extracted from the stimulation sites of patient 03. Especially a stimulation current of 6 mA allows, with respect to the observed reflectance change amplitudes, a differentiation between both groups for this patient. Therefore, at least this stimulation amplitude or higher stimulation current should be used in further investigations. Third-order polynomials were chosen because they are simple to implement and because they allow the modeling of the actual stimulation-induced CBV decrease and increase as well as a possible late overshoot. Future work should concentrate on the implementation and evaluation of advanced modeling approaches for time course analysis, e.g. the dynamic linear modeling mentioned in [6].

Due to the fact that the calculated difference images reveal an activated area that is shifted asymmetrically from the electrode tips, the ROI-based approach for the time course and time course feature extraction should be replaced by more sophisticated analysis methods. Approaches based on the identification of regions with statistically significant differences seem more appropriate. They would hold the advantage that the amplitude of the reflectance changes is not artificially reduced by averaging over regions that are obviously not responding to the stimulus.

The time-resolved analysis of the data from patient 03 revealed that, in contrast to the time courses for the 6 mA stimulation current, which peaked about 25 s after the end of stimulation, the spatial extent of the affected area was already at its maximum for the first calculated difference frame, which was created from data up to 15 s after the end of stimulation. A further increase in the extent of the stimulation-affected area is not visible. With respect to the differentiation between tumor and non-tumor tissue, this result might be useful in the future: it can be utilized to reduce, on the one hand, the region of interest, where time-resolved data should be analyzed and processed in depth. On the other hand, it may allow a reduction in the intraoperative recording time if future research reveals that parameters of the reflectance change time course are not relevant for the initial task of tissue differentiation. Even though the results of this work are encouraging, there are limitations and shortcomings in this study and its underlying methodology that should be taken into account for the future. One of those is the hitherto weak data basis. Measurements were performed on only three patients. Only one technical parameter, the stimulation current, was altered in one patient. Therefore, a statistically reliable evaluation has not yet been possible. Furthermore, optical imaging is due to the low tissue penetration depth of light susceptible to changes in the cortical surface properties. Therefore, even physiological alterations, like a thickened arachnoid, may lead to a weakened signal and a misinterpretation of the measurements. The influence of the tumor localization with respect to the cortical surface and the stimulation site should be highlighted, as well as the influence of the exact tumor pathology and the influence of the microanatomy of different cortical regions.

Conclusion

The results of this study support the notion that differentiation between different brain tissue types might be possible by using optical imaging in connection with direct cortical stimulation. In this first investigation, significant differences between tumor and non-tumor tissue were observed in three patients. The reaction to direct electrical stimulation of non-tumor as well as tumor tissue was analyzed in one patient in detail and the reaction to different stimulation currents was characterized. The method holds the potential to evolve with further research into a clinical tool that provides the surgeon during the tumor

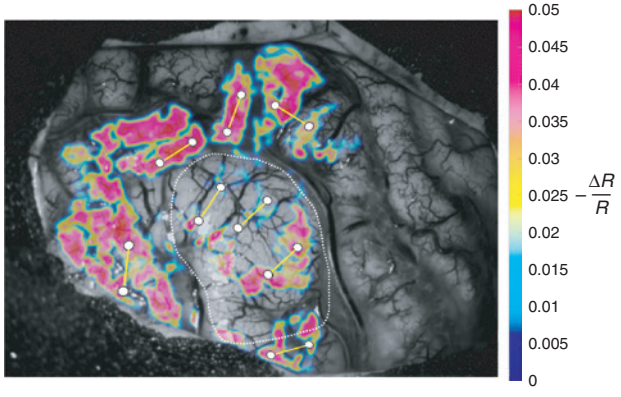

Figure 7: Composite image of all relative difference images for bipolar stimulation performed in patient 02.
Dotted line represents the tumor segmentation border. All stimulations were performed with $I_{Stim} = 6$ mA.

resection with additional valuable information about functionality and pathology of exposed cortical regions. Therefore, further investigations are mandatory. Figure 7 finally gives an impression of how a two-dimensional map can sum up the stimulation answers at different cortical stimulation sites. The map was created immediately after the DCS mapping procedure and might serve as an additional intraoperative tool for the neurosurgeon.

Acknowledgments: This work was financially supported by Carl Zeiss Meditec AG, Oberkochen.

References

[1] Borchers S, Himmelbach M, Logothetis N, Karnath H-O. Direct electrical stimulation of human cortex – the gold standard for mapping brain functions? Nat Rev Neurosci 2012; 13: 63–70.

[2] Desmurget M, Song Z, Mottolese C, Sirigu A. Re-establishing the merits of electrical brain stimulation. Trends Cogn Sci 2013; 17: 442–449.

[3] Frangi AF, Niessen WJ, Vincken KL, Viergever MA. Multiscale vessel enhancement filtering. In: Wells WM, Colchester A, Delp S, editors. Medical image computing and computer-assisted intervention — MICCAI'98. MICCAI 1998. Lecture Notes in Computer Science, vol. 1496, Springer: Berlin, Heidelberg 1998.

[4] Haglund MM, Ojemann GA, Hochman DW. Optical imaging of epileptiform and functional activity in human cerebral cortex. Nature 1992; 358: 668–671.

[5] Haglund MM, Ojemann GA, Blasdel GG. Optical imaging of bipolar cortical stimulation. J Neurosurg 1993; 78: 785–793.

[6] Lavine M, Haglund MM, Hochman DW. Dynamic linear model analysis of optical imaging data acquired from the human neocortex. J Neurosci Methods 2011; 199: 346–362.

[7] Meyer T, Sobottka SB, Kirsch M, et al. Intraoperative optical imaging of functional brain areas for improved image-guided surgery. Biomed Tech (Berl) 2013; 58: 225–236.

[8] Meyer T, Morgenstern U, Kirsch M, Schackert G, Sobottka S. Intraoperative Optical Imaging of intrinsic signals for delineation of active functional brain areas. In: Nabavi A, Samii A, Fahlbusch R, editors. Visualization of the brain and its pathologies – technical and neurosurgical aspects. Der Andere Verlag 2016. ISBN/EAN: 9783862475773. 175–92.

[9] Sanai N, Berger MS. Glioma extent of resection and its impact on patient outcome. Neurosurgery 2008; 62: 753–766.

[10] Senft C, Bink A, Franz K, Vatter H, Gasser T, Seifert V. Intraoperative MRI guidance and extent of resection in glioma surgery: a randomised, controlled trial. Lancet Oncol 2011; 12: 997–1003.

[11] Sobottka SB, Meyer T, Kirsch M, et al. Evaluation of the clinical practicability of intraoperative optical imaging comparing three different camera setups. Biomed Tech (Berl) 2013; 58: 237–248.

[12] Sobottka SB, Meyer T, Kirsch M, et al. Intraoperative optical imaging of intrinsic signals: a reliable method for visualizing stimulated functional brain areas during surgery: clinical article. J Neurosurg 2013; 119: 853–863.

[13] Stieglitz LH, Fichtner J, Andres R, et al. The silent loss of neuronavigation accuracy: a systematic retrospective analysis of factors influencing the mismatch of frameless stereotactic systems in cranial neurosurgery. Neurosurgery 2013; 72: 796–807.

[14] Stummer W, Reulen H-J, Meinel T, et al. Extent of resection and survival in glioblastoma multiforme: identification of and adjustment for bias. Neurosurgery 2008; 62: 564–576.

[15] Suh M, Bahar S, Mehta AD, Schwartz TH. Blood volume and hemoglobin oxygenation response following electrical stimulation of human cortex. Neuroimage 2006; 31: 66–75.

[16] Thirion J-P. Image matching as a diffusion process: an analogy with Maxwell's demons. Med Image Anal 1998; 2: 243–260.